Journal of The
Electrochemical Society

OPEN ACCESS

Thermal Stability Comparison of $LiFePO_4$/Graphite and $LiMn_{0.6}Fe_{0.4}PO_4$/Graphite Pouch Cells using Accelerating Rate Calorimetry

To cite this article: Chanmonirath (Michael) Chak *et al* 2025 *J. Electrochem. Soc.* **172** 090532

View the article online for updates and enhancements.

You may also like

- Electrochemical Properties of $Li_4Ti_5O_{12}$ Coated $LiMn_{0.6}Fe_{0.4}PO_4$ Prepared by Rheological Phase Reaction Method
Haoyan Gu, Weida Li, Quanchen Li et al.
- High Energy Density Flake-Type $LiMn_{0.8}Fe_{0.2}PO_4$
Moarij A. Syed, Mina Salehabadi, Laurie Carrier et al.
- $LiNi_{0.5}Co_{0.2}Mn_{0.3}O_2$-$LiMn_{0.6}Fe_{0.4}PO_4$ Mixture with Both Excellent Electrochemical Performance and Low Cost as Cathode Material for Power Lithium Ion Batteries
Xinxin Zhao, Liwei An, Jiachen Sun et al.

Your Lab in a Box!

EL-CELL® electrochemical test equipment

The PAT-Tester-i-16 Multi-Channel Potentiostat for Battery Material Testing!

- All-in-One Solution with Integrated Temperature Chamber (+10 to +80 °C)!
No additional devices are required to measure at a stable ambient temperature.
- Fully Featured Multi-Channel Potentiostat / Galvanostat / EIS!
Up to 16 independent battery test channels, no multiplexing.
- Ideally Suited for High-Precision Coulometry!
Measure with excellent accuracy and signal-to-noise ratio.
- Small Footprint, Easy to Setup and Operate!
Cableless connection of 3-electrode battery test cells. Powerful EL-Software included.

Learn more on our product website: Scan me!

Download the data sheet (PDF): Scan me!

Or contact us directly:
+49 40 79012-734
sales@el-cell.com
www.el-cell.com

This content was downloaded from IP address 152.23.102.108 on 29/01/2026 at 12:19

Journal of The Electrochemical Society, 2025 **172** 090532

Thermal Stability Comparison of $LiFePO_4$/Graphite and $LiMn_{0.6}Fe_{0.4}PO_4$/Graphite Pouch Cells using Accelerating Rate Calorimetry

Chanmonirath (Michael) Chak,[1,2,3,*] Vadim Shipitsyn,[1,2,3] and Lin Ma[1,2,3,,z]**

[1]*Department of Mechanical Engineering and Engineering Science, University of North Carolina at Charlotte, Charlotte, North Carolina 28223, United States of America*
[2]*Battery Complexity, Autonomous Vehicle and Electrification (BATT CAVE) Research Center, University of North Carolina at Charlotte, Charlotte, North Carolina, 28223, United States of America*
[3]*Department of Applied Physical Sciences, University of North Carolina at Chapel Hill, Chapel Hill, North Carolina, 27514, United States of America*

$LiMn_{0.6}Fe_{0.4}PO_4$ has attracted attention as a promising, high-energy, and cost-effective alternative to $LiFePO_4$ (LFP) for lithium-ion batteries. However, its thermal stability, especially at full cell level, remains less understood compared to LFP. This study compares the cycling performance and thermal stability of $LiMn_{0.6}Fe_{0.4}PO_4$/graphite and LFP/graphite pouch cells using a consistent electrolyte formulation: 1.2 m lithium bis(fluorosulfonyl)imide (LiFSI) in ethylene carbonate (EC):ethyl methyl carbonate (EMC): dimethyl carbonate (DMC) (25:5:70 by volume) with 2 wt% vinylene carbonate (VC). Thermal stability was evaluated with two 250 mAh pouch cells through accelerating rate calorimetry at elevated temperatures. After roughly 275 cycles at C/3 and 40 °C, the LFP/graphite cells retained 91% of their initial capacity, while LMFP/graphite cells retained 89%, indicating slightly better electrochemical stability for LFP cells. Exothermic reactions in LMFP cells initiated around 125 °C, compared to 140 °C for LFP, implying higher thermal vulnerability. Despite this, both cell types exhibited similar self-heating rates below 0.1 °C min^{-1}, demonstrating strong safety performance. Overall, although LMFP offers a higher voltage window, its thermal stability and cycling performance still slightly lag behind LFP.

© 2025 The Author(s). Published on behalf of The Electrochemical Society by IOP Publishing Limited. This is an open access article distributed under the terms of the Creative Commons Attribution 4.0 License (CC BY, https://creativecommons.org/licenses/by/4.0/), which permits unrestricted reuse of the work in any medium, provided the original work is properly cited. [DOI: 10.1149/1945-7111/ae08f2]

Manuscript submitted August 8, 2025; revised manuscript received September 8, 2025. Published September 26, 2025.

Supplementary material for this article is available online

The growing demand for lithium-ion batteries (LIBs) to support the expanding electric vehicle (EV) market has highlighted the need to develop cost-effective battery technologies based on Earth-abundant raw materials.[1] Currently, most EVs utilize either $LiNi_xMn_yCo_{1-x-y}O_2$ (NMC) or $LiFePO_4$ (LFP) as the cathode material.[2] NMC offers higher energy density, making it more suitable for long-range applications; however, it relies on critical transition metals such as nickel (Ni) and cobalt (Co), which are both scarce and expensive.[3] In contrast, LFP is more economically viable due to its use of iron (Fe), which is a highly abundant element. However, LFP's lower operating voltage (3.35 V)[4] result in reduced energy density compared to NMC, which currently hinders LFP from reaching the energy density levels required for broader applications.

$LiMn_xFe_{1-x}PO_4$ has gained attention as a potential alternative to LFP, having been discovered concurrently and sharing the same olivine crystal structure.[4] In this material, partial substitution of Fe is replaced with manganese (Mn) introduces the Mn^{2+}/Mn^{3+} redox couple, which operates at a higher potential than the Fe^{2+}/Fe^{3+} redox couple, leading to an additional voltage plateau during electrochemical cycling.[5,6] As a result, $LiMn_xFe_{1-x}PO_4$ exhibits improved energy density relative to LFP. At the same time, Mn is an abundant and cost-effective element, allowing $LiMn_xFe_{1-x}PO_4$ to offer enhanced performance while maintaining low material and battery costs compared to other high-voltage cathode alternatives. Especially both LFP and $LiMn_xFe_{1-x}PO_4$ cathodes demonstrated excellent thermal stability under high-temperature conditions during accelerating rate calorimetry (ARC) testing at material level.[7] However, despite these advantages, the safety of $LiMn_xFe_{1-x}PO_4$ is still uncertain compared to LFP at full cell level, highlighting the importance of further investigation.

At the cell level, ARC testing remains important for assessing the overall thermal safety of battery systems and understanding the complex interactions among electrodes, electrolytes, and other components under thermal stress. Several studies have leveraged this approach to compare the thermal behavior of LIBs and sodium-ion batteries (SIBs). Carter et al.[8] evaluated three commercial SIBs representing key cathode chemistries: polyanion (Na-VPF), layered metal oxide (Na-NMF), and a Prussian blue analog (Na-tmCN), benchmarking against conventional LIBs, specially LFP and NCA. Their results ranked the safety performance of these cells in the following order: Na-tmCN < Na-VPF < LFP < Na-NMF < NCA. Similarly, Chak et al.[9] studied the thermal stability of $Na_{0.97}Ca_{0.03}[Mn_{0.39}Fe_{0.31}Ni_{0.22}Zn_{0.08}]O_2$ (NCMFNZO)/hard carbon (HC) pouch cells using ARC across different fluoroethylene carbonate (FEC) additive concentrations and state of charge (SOC). Their study also compared these SIB cells with conventional LIB configurations, including LFP/graphite and NMC811/graphite + SiO_x pouch cells. The results showed that NCMFNZO/HC pouch cells demonstrate inferior thermal stability compared to LFP/graphite pouch cells, while NMC811/graphite + SiO_x pouch cells exhibit the worst safety performance, with the highest self-heating rate (SHR) across the entire temperature range. In addition, Zhang et al.[10] investigated the effect of calendar aging on the thermal safety of 4.6 Ah $LiMn_2O_4$ pouch cells using a battery test calorimetry (equivalent to ARC) and found that thermal safety improves after aging at 55 °C and 100% SOC, with a higher onset temperature of SHR and a reduced SHR. Together, these findings highlight the pressing need for ARC testing to be extended to comparisons between LFP and $LiMn_xFe_{1-x}PO_4$ at the cell level, particularly after formation and after long-term cycling, to better assess their thermal safety characteristics and support the development of safer materials for next-generation battery systems.

In this work, we began by evaluating the cell electrochemical performance of $LiMn_{0.6}Fe_{0.4}PO4$ (LMFP)/graphite and LFP/graphite pouch cells. Subsequently, we assessed the thermal stability of these cells at 100% SOC using ARC under elevated temperatures from 50 °C to 315 °C. The safety performance of the pouch cells was compared both after formation and after long-term cycling. Although both LMFP/

*Electrochemical Society Member.
**Electrochemical Society Student Member.
[z]E-mail: L.ma@unc.edu

graphite and LFP/graphite cells demonstrated comparable and inherently safe thermal behavior, the LFP/graphite cells exhibited superior electrochemical performance over extended cycling.

Experimental

Pouch cells.—Machine-made 250 mAh $LiMn_{0.6}Fe_{0.4}PO4$ (LMFP)/graphite pouch cells and 250 mAh $LiFePO_4$ (LFP)/graphite pouch cells, without electrolyte (dry), were obtained from Lifun Technology (Zhuzhou, Hunan, China). In LMFP/graphite pouch cells, the cathode is composed of 93 wt% LMFP active material, 2.6 wt% carbon black, and 4.4 wt% PVDF binder, while the anode consists of 95.7 wt% graphite active material, 3 wt% carboxymethyl cellulose/styrene-butadiene rubber (CMC/SBR) binder, and 1.3 wt% carbon black. The areal loadings of the cathode and anode are 13.53 mg cm^{-2} and 6.05 mg cm^{-2}, respectively. In LFP/graphite pouch cells, the cathode is composed of 96.5 wt% LFP active material, 1.5 wt% carbon black, and 2 wt% PVDF binder, while the anode consists of 95.7 wt% graphite active material, 3 wt% CMC/SBR binder, and 1.3 wt% carbon black. The areal loadings of the cathode and anode are 17.03 mg cm^{-2} and 8.51 mg cm^{-2}, respectively. In both cell types, copper was used as the anode current collector, aluminum was used as the cathode current collector, and 16 μm polyethylene (PE) + 4 μm ceramic coating was used as the separator. The dimensions were $29 \times 19 \times 5.5$ mm for LMFP/graphite pouch cell and $29 \times 19 \times 4.65$ mm for LFP/graphite pouch cell.

Electrolyte preparation.—The electrolyte was prepared in an Ar-filled glovebox (oxygen and water content < 0.01 ppm), and all the electrolyte components were obtained from Shenzhen CapChem (China). 1.2 m lithium bis(fluorosulfonyl)imide (LiFSI) in ethylene carbonate (EC): ethyl methyl carbonate (EMC): dimethyl carbonate (DMC) (25:5:70 by volume) + 2 wt% vinylene carbonate (VC) was used as the main electrolyte in all the pouch cells used in this study. LiFSI was chosen for its superior cycling performance relative to $LiPF_6$-based formulations and to reduce the risk of HF formation from PF_6^- hydrolysis in the presence of trace moisture.[11,12]

Pouch cell filling.—All pouch cells were filled in an Ar-filled glovebox with 1 g of electrolyte and vacuum-sealed using a compact vacuum sealer (MSK-115A-111, MTI Corp.) under a pressure gauge of −90 kPa with a sealing temperature of 165 °C and a sealing time of 5 s.

Formation and cycling.—After filling the electrolyte, all pouch cells were transferred to temperature-controlled chambers (Neware Battery Testing system, China) set at 40 ± 0.1 °C. A single formation cycle was performed on Neware Battery Testing system (China), where cells were charged to 1.5 V, held for 12 h to ensure proper wetting, then charged at C/20 to 3.65 V for LFP/graphite cells and 4.2 V for LMFP/graphite cells. LFP/graphite and LMFP/graphite cells were then discharged to 2.5 V and 3 V, respectively, using C/20 for degas. Subsequently, cells were put into long-term cycling at 40 °C over a voltage range of 2.5–3.65 V for LFP/graphite cells and 3–4.2 V for LMFP/graphite cell. All cells were cycled using constant current constant voltage (CCCV) charge and constant current (CC)

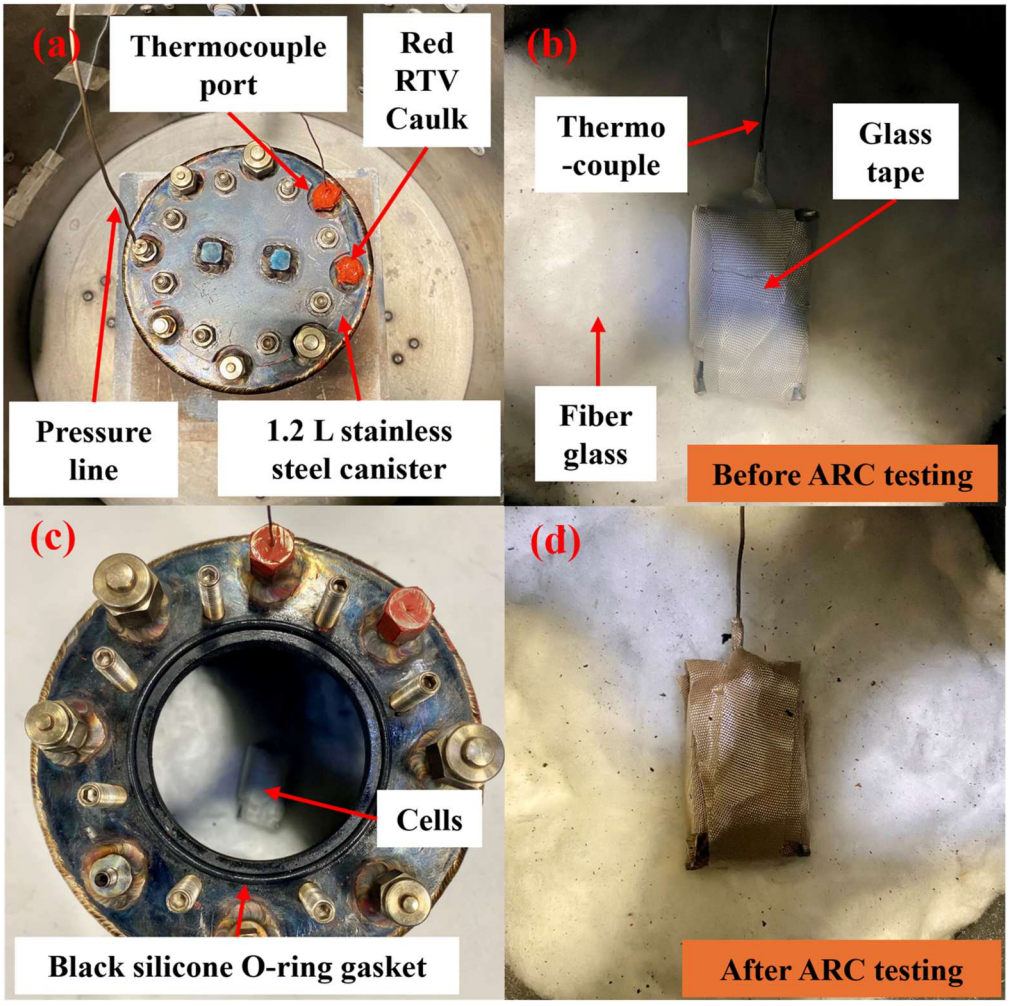

Figure 1. A summary of steps on how to set up an ARC test with canister for pressure measurement (a)–(c). Photograph of a pair of pouch cells after ARC test (d).

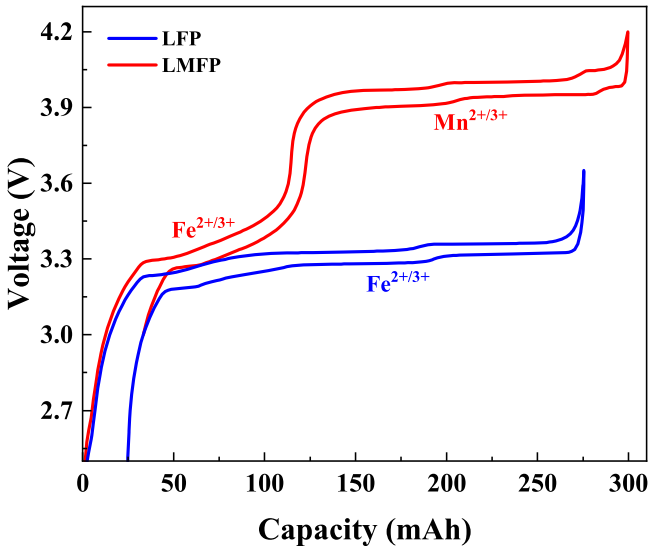

Figure 2. Voltage vs capacity curves during formation with active transition metal redox labeled for each region of LMFP/graphite (red) and LFP/graphite (blue) pouch cell.

discharge at a C/3 rate. The cut-off current of the CV held on charge was C/10. A C/20 check-up cycle was performed every 50 cycles.

Gas measurement.—The amount of gas generated in the pouch cells during formation and cycling was determined through the application of Archimedes' principle, as detailed in the work by Aiken et al.[13]

Electrochemical impedance spectroscopy (EIS) test.—EIS measurements were conducted in both cell types at 50% SOC after formation and after long-term cycling, for EIS measurement. Th EIS data was collected using a BioLogic VMP3, involved ten data points per decade within the frequency range of 100 kHz to 100 mHz. The signal amplitude was set at 10 mV, and the measurements were conducted at 10 °C. Figure S1 shows the equivalent circuit models used to fit impedance spectra in this paper. Fits were completed using ZFit software.

Scanning electron microscopy (SEM).—SEM images of fresh LMFP and graphite electrodes were acquired using JEOL JSM-6480 instrument (JEOL, Japan), as shown in Fig. S2. Electrons were generated using a Tungsten (W) filament and the SEM was operated in secondary electron analysis mode with an accelerating voltage of 20 kV.

Accelerating rate calorimetry (ARC) measurement.—In this study, an accelerating rate calorimeter (EV+ ARC, Thermal Hazard Technology) was employed to investigate the thermal stability of the pouch cells, both after formation and after cycling at elevated temperatures. A 1.2 L stainless steel canister was used in conjunction with the ARC to monitor pressure evolution during testing. A type-N thermocouple was inserted through the thermocouple port, sealed with a piece of red RTV silicone between the thermocouple nut and the port to prevent leakage (Fig. 1a). To minimize conductive heat transfer from the cells to the canister, a layer of glass fiber insulation was placed at the base of the canister. During each experiment, two pouch cells at 100% SOC were positioned around the thermocouple using glass tape (Fig. 1b). A black silicone O-ring was placed between the canister and its lid to ensure a gas-tight seal, while any unused ports were sealed with

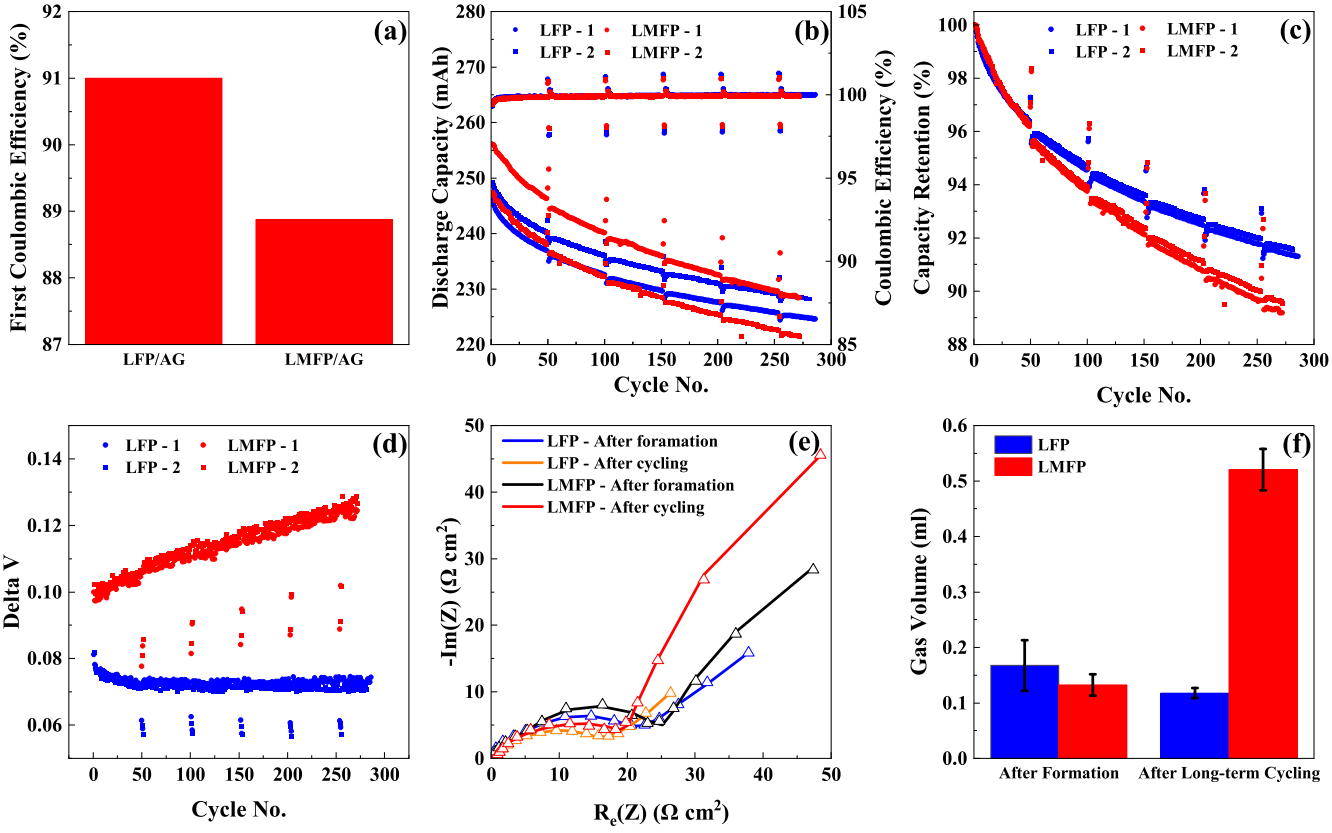

Figure 3. Evaluation of electrochemical performance of LMFP/graphite and LFP/graphite pouch cells. First-cycle coulombic efficiency (a), discharge capacity and coulombic efficiency (b), capacity retention (c), and delta V (d) vs cycle number cycled over a voltage range of 2.5–3.65 V for LFP/graphite pouch cells and 3–4.2 V for LMFP/graphite pouch cells at a rate of C/3 with a C/20 for every 50 cycles. Nyquist plot measured at 50% SOC and 10 °C (e), and gas volume (f) of both cell types after formation and after long-term cycling. Each cell type has two identical cells for the cycling tests. In (e), triangles denote fitted data while the solid line shows the experimental data. The equivalent circuit used for fitting is presented in Fig. S1.

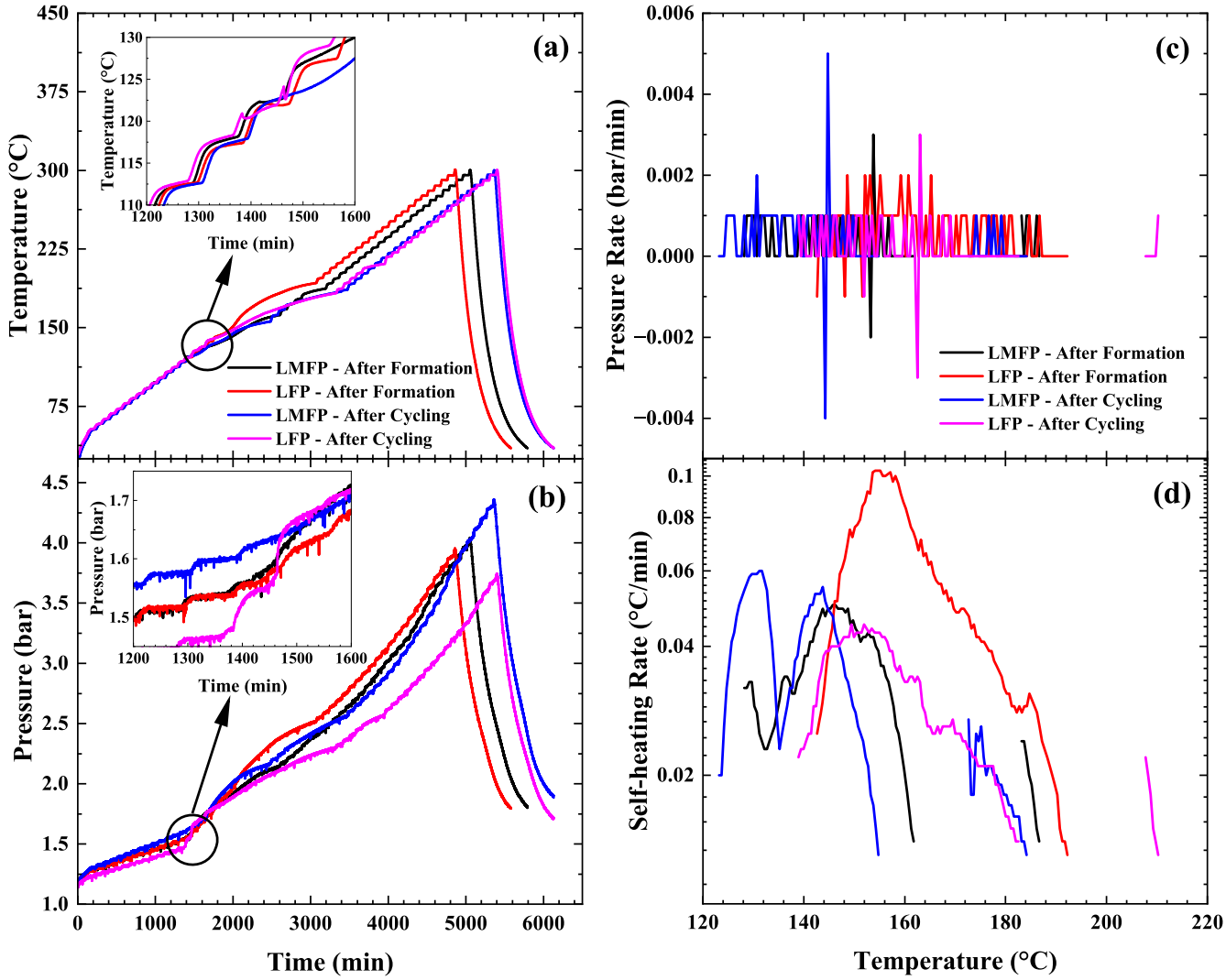

Figure 4. Temperature (a) and pressure (b) vs time, and pressure rate (c) and self-heating rate (SHR) (d) vs temperature for LFP/graphite and LMFP/graphite pouch cells, both after formation and after cycling. Each ARC test was conducted using two 100% SOC pouch cells. The discontinuity in (d) results from plotting only exothermic regions where the SHR exceeds the threshold (0.02 °C min^{-1}).

stainless steel nuts (Fig. 1c). Additional red RTV silicone was applied to the thermocouple nut area on the exterior of the canister for improved high-temperature sealing. A pressure transducer was connected to the canister via a pressure line to allow real-time pressure monitoring outside the ARC calorimetry (Fig. 1a). Throughout the testing period, the thermocouple remained centered between the two pouch cells to provide accurate internal temperature measurements (Fig. 1d). ARC tests were conducted over a temperature range of 50 °C to 315 °C using the heat-wait-search (HWS) mode, with temperature increments of 5 °C and a 60 min waiting time at each step. Once the sample's SHR surpassed 0.02 °C min^{-1}, the system automatically transitioned to exothermic mode to maintain adiabatic conditions.

Results and Discussion

Figure 2 shows the voltage profile of LMFP/graphite and LFP/graphite pouch cells during the formation cycle, with the respective voltage ranges and redox couples indicated. The Mn^{2+}/Mn^{3+} redox couple in LMFP occurs at a higher potential compared to the Fe^{2+}/Fe^{3+} redox in LFP, and this higher voltage plateau can potentially provide LMFP with a higher energy density. By integrating the voltage vs capacity curve of a single LMFP/graphite and LFP/graphite pouch cell during the formation cycle, the gravimetric and volumetric energy densities were calculated. The LMFP/graphite pouch cell exhibited a gravimetric energy density of 169 Wh kg^{-1} and a volumetric energy density of 360 Wh l^{-1}, while the LFP/graphite pouch cell showed slightly lower values, with a gravimetric energy density of 154 Wh kg^{-1} and a volumetric energy density of 355 Wh L^{-1}. Despite an initial charging capacity of 300 mAh for LMFP/graphite and 275 mAh for LFP/graphite pouch cell, irreversible capacity-loss leads to a reversible capacity of 250 mAh in both cell types. Therefore, we stated that ARC testing was carried out on two 250 mAh pouch cells in this study.

The electrochemical performance of LMFP/graphite and LFP/graphite pouch cells was evaluated by calculating first coulombic efficiency (FCE) (Fig. 3a), long-term cycling (Figs. 3b–3d), charge transfer resistance (R_{ct}) (Fig. 3e), gas volume evolution (Fig. 3f). The FCE was determined to be 88.88% for the LMFP/graphite and 91% for the LFP/graphite pouch cell (Fig. 3a). During the long-term cycling, the pouch cells were cycled over a voltage range of 3–4.2 V and 2.5–3.65 V for LMFP/graphite and LFP/graphite, respectively, at 40 °C and C/3 with C/20 check-up cycles every 50 cycles. Each cell type was tested in duplicate. Figure 3b shows the discharge capacity

and coulombic efficiency (CE) as a function of cycle number. In Fig. 3c, all the discharge capacity was normalized based on the discharge capacity of the first cycle using C/3. Both cell types performed comparably until 50 cycles, after which LMFP/graphite cells began to show accelerated capacity fade. The "C/20 checking" cycling revealed that LMFP/graphite cells started to decline more noticeably than LFP/graphite cells after around 150 cycles. By 275 cycles, the LFP/graphite cells retained 91% of their initial capacity, while LMFP/graphite cells retained 89% of their initial capacity, indicating a better electrochemical performance for LFP/graphite cells. The poorer cycling performance of LMFP/graphite cells could primarily be attributed to lattice distortion induced by Jahn-Teller active Mn^{3+}, which hinders Li^+ diffusion and substantially increases voltage polarization (Fig. 3d). The delta V (Fig. 3d) is the difference between the average charge and the average discharge voltage, which indicates voltage polarization growth during cycling. Consistently, LMFP/graphite cells exhibited a steady increase in delta V over time, while LFP/graphite cells maintained a nearly constant delta V.

According to the Nyquist plot with equivalent circuit fitting (Figs. 3e, S1), the R_{ct} of LMFP/graphite cell (14.19 $\Omega{\cdot}cm^2$) was higher than the LFP/graphite cell (7.94 $\Omega{\cdot}cm^2$) during the formation. After long-term cycling, both cell types exhibited increased R_{ct} values; however, the LMFP/graphite cell showed a significantly higher post-cycling R_{ct} (112.2 $\Omega{\cdot}cm^2$) than the LFP/graphite cell (69.52 $\Omega{\cdot}cm^2$), consistent with the trend observed in Fig. 3d. In addition, gas volume evolution (Fig. 3f) revealed that while the LFP/graphite cell produced slightly more gas during the formation stage, the LMFP/graphite cell generated a considerably larger gas volume during the long-term cycling.

ARC experiments were conducted to assess the thermal stability of LMFP/graphite and LFP/graphite pouch cells using identical electrolyte composition, separator material, and comparable capacities for both after formation (fresh) and after cycling (aged) cases. Each ARC experiment was done with two 100% SOC pouch cells, corresponding to a total capacity of approximately 500 mAh for the fresh cell tests and 450 mAh for the aged cell tests. Figure 4 reveals the thermal characteristics of both fresh and aged LFP/graphite and LMFP/graphite pouch cells. Early signs of small venting were observed at approximately 120 °C in all cells, as evidenced by sharp inflections in the temperature profile (Fig. 4a) and a modest rise in pressure around the 1400 min mark (Fig. 4b). Notably, there were no abrupt pressure changes observed throughout the tests (Fig. 4c). Additionally, this gradual pressure rise is primarily attributed to the external heating rather than internal venting from the cells. SHR onset temperatures, defined as the temperature at which the SHR first exceeds 0.02 °C min^{-1}, differed between the two cell types. LMFP/graphite cells exhibited an earlier onset at 125 °C, whereas LFP/graphite cells demonstrated a higher onset temperature of 140 °C (Fig. 4d), suggesting slighly better thermal stability for the LFP/graphite system. At the same time, slight decrease in onset temperature was observed for both cell types after cycling. Despite these variations, the SHR of all cells (i.e., fresh and aged cells) remained below 0.1 °C min^{-1} throughout the entire test range, indicating minimal exothermic reactivity and confirming the superior thermal safety characteristics of both LFP/graphite and LMFP/graphite systems. Please note that this study used lab-scale pouch cells and duplicate experiments to establish preliminary datasets for comparing the thermal stability of LFP/graphite and LMFP/graphite cells. Larger, statistically powered test sets are required in future work to further distinguish intrinsic chemistry effects from sample-to-sample variation, particularly for larger format cells (>100 Ah) that are representative of grid and vehicle applications. We also note a limitation of the canister-style ARC setup used here: for cells with low SHR, the canister could absorb heat and alter the apparent thermal response. This artifact can be mitigated by using a closed ARC configuration (i.e. loading the cell into a fully sealed ARC chamber rather than a canister inside a chamber), which enables accurate, simultaneous measurement of gas-evolution rate and SHR.

Conclusions

In this study, a detailed comparison of the electrochemical performance and thermal stability of LFP/graphite and LMFP/graphite pouch cells was conducted under identical testing conditions. Through EIS, gas evolution analysis, and long-term cycling tests, it was observed that LMFP/graphite cells exhibited faster performance degradation compared to their LFP/graphite counterparts. This could primarily be due to additional degradation mechanisms specific to LMFP, including Jahn-Teller distortion from Mn^{3+} and Mn dissolution during cycling, which led to higher impedance and greater lithium inventory loss. The thermal behavior of the cells was also investigated using ARC. While all cells demonstrated excellent safety performance, with SHR remaining below 0.1 °C min^{-1} across the entire test range, LMFP/graphite cells exhibited slightly lower SHR onset temperatures for thermal reactivity compared to LFP/graphite cells, in both fresh and aged states. This suggests that LMFP is slightly more prone to thermal reactions under elevated temperatures, although still within a safe range.

This work provides side-by-side comparisons of LFP and LMFP chemistries at the pouch cell level using graphite as the anode, delivering valuable insight into the practical implications of adopting LMFP in commercial systems. Although LMFP offers advantages such as a higher voltage window and potentially greater energy density, its cycling durability and thermal robustness remain slightly inferior to those of the well-established LFP system. These findings emphasize the importance of addressing the intrinsic material limitations of LMFP, particularly transition-metal dissolution and interphasial instability, to fully realize its potential. Future research should focus on electrolyte optimization, cathode surface engineering, and advanced cell design strategies to improve the long-term stability, safety, and commercial viability of LMFP-based lithium-ion batteries.

Acknowledgments

Lin Ma acknowledges the support of the US National Science Foundation Award No. 2301719.

ORCID

Lin Ma https://orcid.org/0000-0003-1183-1347

References

1. Y. Deng, C. Yang, K. Zou, X. Qin, Z. Zhao, and G. Chen, "Recent advances of Mn-Rich $LiFe_{1-y}Mn_yPO_4$ ($0.5 \leqslant y < 1.0$) cathode materials for high energy density lithium ion batteries." *Adv. Energy Mater.*, **7**, 1601958 (2017).
2. H. Kim, S. M. Oh, B. Scrosati, and Y. K. Sun, "9 - High-performance electrode materials for lithium-ion batteries for electric vehicles." *Advances in Battery Technologies for Electric Vehicles*, ed. B. Scrosati et al. (Woodhead Publishing) 191 (2015).
3. H.-H. Ryu, H. H. Sun, S.-T. Myung, C. S. Yoon, and Y.-K. Sun, "Reducing cobalt from lithium-ion batteries for the electric vehicle era." *Energy Environ. Sci.*, **14**, 844 (2021).
4. A. K. Padhi, K. S. Nanjundaswamy, and J. B. Goodenough, "Phospho-olivines as positive-electrode materials for rechargeable lithium batteries." *J. Electrochem. Soc.*, **144**, 1188 (1997).
5. A. Yamada and S.-C. Chung, "Crystal chemistry of the olivine-type Li (Mn_yFe_{1-y}) PO_4 and (Mn_yFe_{1-y}) PO_4 as Possible 4 V cathode materials for lithium batteries." *J. Electrochem. Soc.*, **148**, A960 (2001).
6. A. Yamada, Y. Kudo, and K.-Y. Liu, "Reaction mechanism of the olivine-type lix ($Mn_{0.6}Fe_{0.4}$) PO_4 ($0 \leqslant x \leqslant 1$)." *J. Electrochem. Soc.*, **148**, A747 (2001).
7. D. Ouyang, Y. Liu, I. Hamam, J. Wang, and J. Dahn, "A comparative study on the reactivity of charged Ni-rich and Ni-poor positive electrodes with electrolyte at elevated temperatures using accelerating rate calorimetry." *Journal of Energy Chemistry*, **60**, 523 (2021).
8. R. Carter, G. H. Waller, C. Jacob, D. Hayman, P. J. West, and C. T. Love, "First look at safety and performance evaluation of commercial sodium-ion batteries." *Energies*, **18**, 661 (2025).
9. C. Chak, R. Jayakumar, V. Shipitsyn, E. Bass, R. McCloskey, W. Zuo, P. M. L. Le, J. Xu, and L. Ma, "Unveiling the thermal stability of sodium ion pouch cells using accelerating rate calorimetry." *J. Electrochem. Soc.*, **171**, 070512 (2024).

10. J. Zhang, L. Su, Z. Li, Y. Sun, and N. Wu, "The evolution of lithium-ion cell thermal safety with aging examined in a battery testing calorimeter." *Batteries*, **2**, 12 (2016).
11. E. R. Logan, A. Eldesoky, E. Eastwood, H. Hebecker, C. P. Aiken, M. Metzger, and J. R. Dahn, "The use of LiFSI and LiTFSI in $LiFePO_4$/Graphite pouch cells to improve high-temperature lifetime." *J. Electrochem. Soc.*, **169**, 040560 (2022).
12. L. Tong, J. Ji, Y. Zhao, L. Wang, and X. He, "The rise of lithium bis(fluorosulfonyl) imide: An efficient alternative to LiPF6 and functional additive in electrolytes." *Mater. Today*, **85**, 282 (2025).
13. C. P. Aiken, J. Xia, D. Y. Wang, D. A. Stevens, S. Trussler, and J. R. Dahn, "An apparatus for the study of in situ gas evolution in li-ion pouch cells." *J. Electrochem. Soc.*, **161**, A1548 (2014).